Journal of Energy Chemistry 37 (2019) 29–34

Contents lists available at ScienceDirect

Journal of Energy Chemistry

journal homepage: www.elsevier.com/locate/jechem

http://www.journals.elsevier.com/journal-of-energy-chemistry/

Lithium–matrix composite anode protected by a solid electrolyte layer for stable lithium metal batteries

Xin Shen[a,1], Xinbing Cheng[a,1], Peng Shi[a], Jiaqi Huang[b,*], Xueqiang Zhang[a], Chong Yan[b], Tao Li[a], Qiang Zhang[a,**]

[a] Beijing Key Laboratory of Green Chemical Reaction Engineering and Technology, Department of Chemical Engineering, Tsinghua University, Beijing 100084, China

[b] Advanced Research Institute of Multidisciplinary Science, Beijing Institute of Technology, Beijing 100081, China

ARTICLE INFO

Article history:
Received 3 November 2018
Revised 28 November 2018
Accepted 29 November 2018
Available online 30 November 2018

Keywords:
Lithium metal anode
Solid electrolyte layer
Composite electrode
Lithium metal dendrites
Rechargeable batteries

ABSTRACT

Lithium (Li) metal with an ultrahigh specific theoretical capacity and the lowest reduction potential is strongly considered as a promising anode for high-energy-density batteries. However, uncontrolled lithium dendrites and infinite volume change during repeated plating/stripping cycles hinder its practical applications immensely. Herein, a house-like Li anode (housed Li) was designed to circumvent the above issues. The house matrix was composed of carbon fiber matrix and affords a stable structure to relieve the volume change. An artificial solid electrolyte layer was formed on composite Li metal, just like the roof of a house, which facilitates uniform Li ions diffusion and serves as a physical barrier against electrolyte corrosion. With the combination of solid electrolyte layer and matrix in the composite Li metal anode, both dendrite growth and volume expansion are remarkably inhibited. The housed Li | $LiFePO_4$ batteries exhibited over 95% capacity retention after 500 cycles at 1.0 C in coin cell and 85% capacity retention after 80 cycles at 0.5 C in pouch cell. The rationally combination of solid electrolyte layer protection and housed framework in one Li metal anode sheds fresh insights on the design principle of a safe and long-lifespan Li metal anode for Li metal batteries.

1. Introduction

Energy storage systems with high energy density have been pursued ceaselessly. The current commercial lithium (Li) ion batteries (LIBs) have achieved impressive advance since released by Sony Corporation in 1991 and dominate a chunk of the portable electronic and electric vehicle markets [1]. However, the practical energy density of LIBs is approaching their theoretical limits with current intercalation chemistry. In light of the ever-growing demands for even higher energy density storage, Li metal batteries (LMBs) have been revisited [2–4]. While replacing the graphite anode of LIBs with Li metal of LMBs, the theoretical energy density of LMBs can be significantly improved due to its ultrahigh specific capacity (3860 mAh g^{-1}) and the lowest redox potential (−3.04 V vs. the standard hydrogen electrode) [5].

However, LMB is still in its infancy. Uncontrolled lithium dendrites and infinite volume change are the main issues. Due to the high reactivity of Li metal, a brittle and uneven solid electrolyte interface (SEI) spontaneously forms on its surface while being exposed to electrolyte [6,7]. The SEI is heterogeneous and induces Li dendrite growth. The dendrite growth can pierce SEI, leading to the side reactions between fresh Li and electrolyte. Moreover, drastic volume change induced by host-less deposition also causes repeated rupture and regeneration of SEI in the subsequent stripping/plating process, which interminably consumes electrolytes and bulk Li and induces low Coulombic efficiency and poor utilization of Li (Fig. 1a) [8]. Therefore, notorious dendrite formation, aggravated side reactions, and infinite relative volume change significantly plague the implementation of Li metal anode by causing short cycle life and potential safety hazards.

Tremendous efforts have been devoted to addressing the above mentioned issues [9–12], mainly focusing on two aspects: (1) Construction of emerging Li matrices. Encapsulating metallic Li in a porous and robust matrix can overcome the volume change issues considerably. Besides, large specific surface area and high conductivity can effectively reduce local current density and thus suppress Li dendrite growth [13,14]. Accordingly, carbon materials

* Corresponding author.
** Corresponding author.
E-mail addresses: jqhuang@bit.edu.cn (J. Huang), zhang-qiang@mails.tsinghua.edu.cn (Q. Zhang).
[1] Both authors contributed equally to this work.

https://doi.org/10.1016/j.jechem.2018.11.016

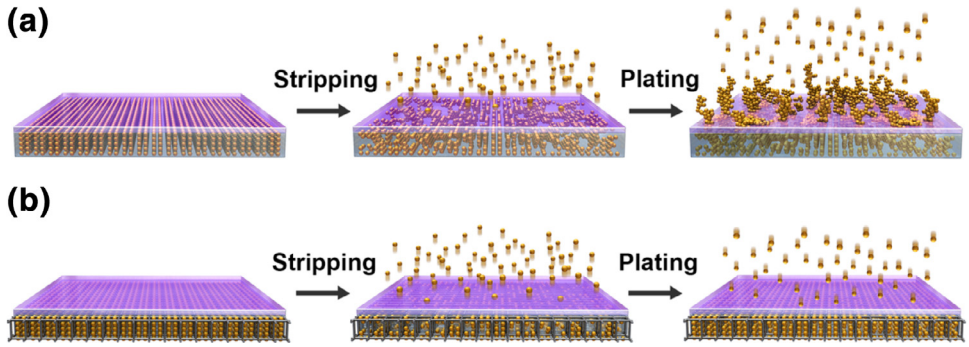

Fig. 1. Schematics of morphology evolution on (a) bare Li and (b) housed Li during stripping/plating cycles.

[15–18], three-dimensional (3D) metal frameworks [19,20], and other novel hosts (e.g., metal–organic frameworks) [21,22], have been introduced as composite Li metal anode. (2) Construction of stable lithium metal interfaces. Various electrolyte additives [23–26], salts [27], solvents [28], highly concentrated electrolytes [29–31], solid electrolyte [32] and artificial SEI [33–35] have been proposed to construct stable SEI on working Li metal anode. Particularly, solid electrolytes, including sulphides [36], oxides [37], polymers [38], and their composites have attracted considerable interests owing to their outstanding merits in inherent safety and wide voltage window [39]. Although the lifespan has been extended by present strategies, yet it is far from the requirement of a practical battery. Generally, the host is expected to suppress dendrite growth and volume change, the solid electrolyte layer can reduce the side reactions and regulate uniform Li deposition [40,41]. If a stable solid electrolyte layer can be created on a 3D Li metal anode, the as-obtained composite Li metal will make much sense for highly safe LMBs.

In this contribution, a composite Li metal anode by the rational design of a Li–matrix anode protected by a solid electrolyte layer was proposed. The composite anode acts similarly as a house to human beings (Fig. S1, Supporting Information). The upper solid electrolyte layer with high mechanical strength and rapid and uniform Li ions diffusion in the housed Li, serves as the roof of a house. The bottom matrix with a robust structure serves as frames of the house, providing rapid electron paths and large interspace for Li deposition (Fig. 1b). Therefore, the composite anode is named housed Li herein. To demonstrate this concept, carbon fibers (CFs), were selected as matrix materials to encapsulate Li metal by roll press. A solid electrolyte layer (SE) was obtained by a facile chemical reaction between copper fluoride (CuF_2)-contained electrolyte and Li metal. Under the synergetic function of matrix and solid electrolyte layer, both Li dendrites and volume expansion were well controlled in housed Li, realizing stable and safe Li metal anode. The symmetrical cell with housed Li metal anode achieved a prolonged cycle time of 1850 h at 0.5 mA cm^{-2} and 950 h at 1.0 mA cm^{-2}. Coupled with $LiFePO_4$ cathodes, the housed Li exhibited over 95% capacity retention after 500 cycles at 1.0 C in coin cell and 85% capacity retention after 80 cycles at 0.5 C in pouch cell.

2. Experimental

2.1. Fabrication of electrodes

The CF papers (Shanghai Hesen Electric, void ratio of 75%) were desiccating by Li foils for 24 h before using. The dried CF papers and two metallic Li foils (thickness: 50 μm, China Energy Lithium Co., Ltd) were sandwiched by rollpress lamination, that was performed in a dry room (relative humidity <0.4% at room temperature). The as-prepared CF/Li was then pouched into shapes and sizes of anodes (13 mm disks for coin cell and 40 mm × 70 mm plates for pouch cell). 5.0 wt% $LiNO_3$ and 1.0 wt% CuF_2 (Alfa Aesar) additives were dissolved in dimethoxyethane solvent (DME, Tokyo Chemical Industry Co., Ltd.) to obtain the precursor electrolyte for in-situ solid electrolyte formation. The in-situ solid electrolyte was fabricated by soaking the anodes into precursor electrolytes for 5 s. A rapid replacement reaction occurs between Li metal and CuF_2 ($CuF_2 + 2Li \rightarrow 2LiF + Cu$). Bare Li with a thickness of 100 μm was adopted as control. Above operations were performed in an Argon-filled glovebox with water and oxygen content less than 1.0 ppm.

The $LiFePO_4$ cathode was prepared by mixing $LiFePO_4$ powders (Shenzhen Kejing Star Technology Co., Ltd.), carbon black, and poly(vinylidene fluoride) at a weight ratio of 80: 10: 10 to form a slurry. Then the slurry was cast on the aluminum foil and dried at 90 °C under air drying for 48 h. The typical active material loading was about 9.0 mg cm^{-2} (1.5 mAh cm^{-2}). The $LiFePO_4$ cathode with an active material loading of 12.0 mg cm^{-2} (2.0 mAh cm^{-2}) each side for pouch cell was acquired from SCM Hypnergy Material Tech Co., Ltd.

2.2. Characterizations

Scanning electron microscopy (SEM) images and corresponding energy-dispersive elemental mapping were acquired by JSM 7401F (JEOL, Japan). Prior to the characterizations, the samples obtained from disassembled cells were first rinsed three times with DME, and then dried in the Ar-filled grove box. X-ray diffraction (XRD) patterns were obtained on a Bruker D8 Advance with a Cu-$K\alpha$ radiation source and 2θ in the range of 5° to 90° at 5° min^{-1}. X-ray Photoelectron Spectroscopy (XPS, ESCALAB 250Xi, Thermo Fisher Scientific, USA) was employed to analyze the composition of the solid electrolyte.

2.3. Electrochemical test

Coin cell CR2025 was used for cell assembly, with Celgard 2400 separator in which an electrolyte amount of 60 μL was deposed. The electrolyte employed in this paper was 1.0 M lithium hexafluorophosphate ($LiPF_6$) in a ternary solvent of fluoroethylene carbonate (FEC), dimethyl carbonate (DMC), and DME (7:7:6 in volume, Alfa Aesar) with 1.1 wt% $LiNO_3$ (Shanghai Aladdin Bio-Chem Technology Co., LTD.) unless otherwise stated (denoted as FEC/$LiNO_3$ electrolyte). Commercial Li-ion battery electrolyte (1.0 M $LiPF_6$ in ethylene carbonate (EC)/diethyl carbonate (DEC) (1:1 in volume)) was purchased from Beijing Institute of Chemical Reagents. Li | Li symmetric cells were assembled for studying the morphology evolution and the electrochemical anodic stability. The cells were tested by a LAND multichannel battery cycler (Wuhan LAND electronics Co., Ltd.). Electrochemical impedance

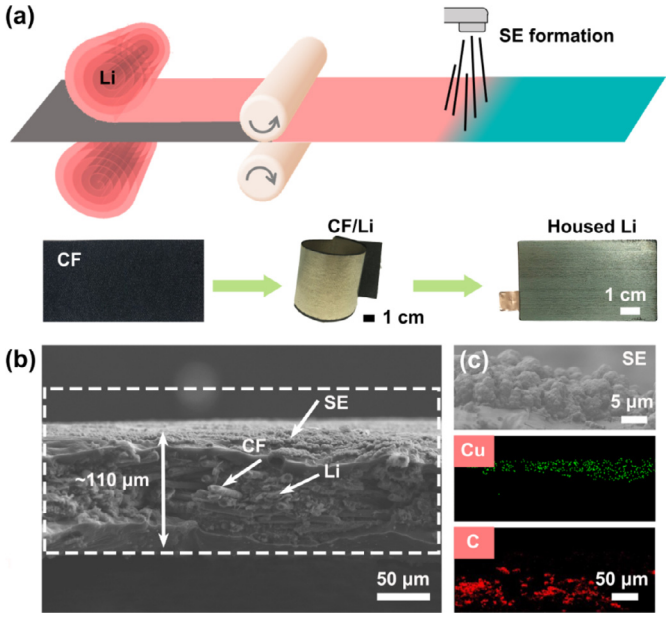

Fig. 2. Fabrication process and morphology characterization of housed Li. (a) Schematic diagram of the fabrication process of housed Li; (b) SEM images of housed Li at the cross-section; (c) Detailed views of solid electrolyte layer and EDS spectrograms of the dash area in (b).

spectroscopy (EIS) was recorded by a Solartron 1470E electrochemical workstation (Solartron Analytical, UK) in a frequency range between 10^5 and 10^{-1} Hz with a voltage amplitude of 10 mV.

The Li | $LiFePO_4$ coin cells were cycled between 2.5 and 4.0 V with charge/discharge rates of 1.0 C (170 mAh g^{-1}, first activated cycle is 0.1 C), corresponding to current density of about 1.5 mA cm^{-2}. The Li | $LiFePO_4$ pouch cells incorporated *n* anode–separator–cathode stacks were also cycled between 2.5 to 4.0 V. They were firstly cycled at 0.05 C for one cycle and then cycled at 0.5 C.

3. Results and discussion

The fabrication of housed Li was realized by a facile method shown in Fig. 2(a). In details, (1) two thin Li foils were firstly incorporated into CF matrix (Fig. S2, Supporting Information) by roll press at room temperature (denoted as CF/Li). (2) The as-prepared CF/Li is processed by a solution of 5.0 wt% $LiNO_3$ and 1.0 wt% CuF_2 in DME to generate an artificial solid electrolyte layer.

The as-obtained housed Li is with a thickness of ca. 110 μm (Fig. 2b). The upper solid electrolyte layer with a thickness of ca. 5 μm (Fig. 2c, top) uniformly covers on the surface of housed Li (Fig. S3, Supporting Information), acting as a physical barrier against electrolyte corrosion. At the bottom layer, Li metal fully fills in the voids of CF and the interconnected structure of CF is well preserved. The areal capacity of housed Li is about 18.75 mAh cm^{-2} (Fig. S4, Supporting Information). Energy dispersive spectroscopy (EDS) mapping images of housed Li (Fig. 2c) further confirm that the SE identified by Cu element covers on the top as a roof, and CF identified by C element acts as a support frame in house.

To characterize the chemical compositions of housed Li, both XRD and XPS were employed. As exhibited by Fig. 3(a), the peak of CF disappears while the peak of LiC_6 arises in the XRD spectra of CF/Li and housed Li, suggesting that CF can be lithiated to LiC_6 at room temperature. It has been demonstrated that LiC_6 is highly electric conductive and compatible with Li metal [42,43]. Thus, a close contact interface between Li and CF can be achieved, contributing to rapid electron transfer in the matrix. There are LiF and Cu in the upper solid electrolyte layer (Fig. 3b, c), which confirms the reactions between Li and CuF_2. Besides, the inorganic components of $LiNO_2$ and LiN_xO_y are also detected due to the additive of $LiNO_3$ in treating solution, which are in accordance with previous reports [44–46].

To explore morphology evolution of the housed Li during plating/stripping cycles, symmetrical cells were assembled and galvanostatically cycled at a current density of 1.0 mA cm^{-2} and a capacity of 1.0 mAh cm^{-2}. The bare Li was also investigated as a control sample in this work. Stocky Li dendrites with inconsistent diameters emerge on the surface of bare Li after the first cycle (Fig. S5a, Supporting Information), rendering enormous risk of a penetrating separator. A pulverized morphology completely different from the initial cycle appears on the surface of bare Li after 10 and 50 cycles due to the accumulation of "dead Li" (Fig. 4a, c). A thickness of ca. 7 μm "dead Li" emerges on the anode surface after 10 cycles (Fig. 4b). After 50 cycles, this layer is completely replaced by rugged and loose "dead Li", increasing to ca. 20 μm (Fig. 4d). With prolonged cycles up to 200 times, the thickness of "dead Li" layer increases to ca. 67 μm (Fig. S5c, Supporting Information). In contrary, the surface of housed Li is flat and compact (Fig. S5b, Supporting Information; Fig. 4e, g). The thickness variation of Li deposition is less than 5 μm after 50 cycles (Fig. 4f, h). Even after 200 cycles, housed Li maintains its integrity and preserves a smooth cross section morphology (Fig. S5d, Supporting Information). XPS analysis was employed to reveal the component of the surface of housed Li after cycles (Fig. S6, Supporting Information). Compared to initial spectrum (Fig. 3), only few peak evolutions are observed, indicating the solid electrolyte layer can maintain stability in the electrochemical environment. Therefore, the housed Li can remarkably alleviate Li dendrites and confine volume change.

The cycling stability was investigated by galvanostatic symmetrical cells with different anodes. At a current of 0.5 mA cm^{-2} and a capacity of 0.5 mAh cm^{-2}, the cell with bare Li exhibits continuously increased voltage hysteresis (over 500 mV after 1600 h cycling), mainly due to the ever-growing dendrites and ever-thickening "dead Li" layer (Fig. S7a, Supporting Information). In contrast, the cell with housed Li displays a lower and more stable hysteresis of 120 mV for more than 1850 h, suggesting uniform Li stripping/plating processes and reduced "dead Li", which is consistent with the morphology observation (Figs. 4 and S5, Supporting Information).

When the current density is increased to 1.0 mA cm^{-2} and the capacity to 1.0 mAh cm^{-2} (Fig. S7b, Supporting Information), the housed Li exhibits a prolonged cycling time of 950 h. Detailed comparison of voltage profiles with bare Li, SE/Li, CF/Li and housed Li is presented in Fig. S7(c) (Supporting Information). The overpotential of symmetrical cells decreases orderly as bare Li, SE/Li, CF/Li and housed Li. When the cells were tested at a graded current from 0.2, 0.5, 1.0, 2.0, to 4.0 mA cm^{-2}, the symmetric cell with housed Li presents stable voltage profiles with much smaller hysteresis than that of bare Li (Fig. S7d, Supporting Information). In particular, housed Li delivers a low overpotential of 0.15 V at 4.0 mA cm^{-2} whereas the overpotential of the bare Li is ca. 0.30 V. It implies that uniform and fast ion/electron channels constructed by solid electrolyte layer and CF matrix are achieved on housed Li.

Electrochemical impedance spectroscopy measurements were carried out to gain insight into the interface variation. The interface resistance can be estimated from the first semi-circle in high-frequency region (Fig. S8, Supporting Information). At the initial state, both the bare Li and housed Li exhibit a similar interfacial resistance of ca. 50 Ω. After cycling, the interfacial resistance of bare Li changes from 18 Ω (1st cycle) to 15 Ω (10th cycles), while the interfacial resistance of housed Li changes from 14 Ω (1st cycle) to 8 Ω (10th cycles). We can infer that the upper solid electrolyte

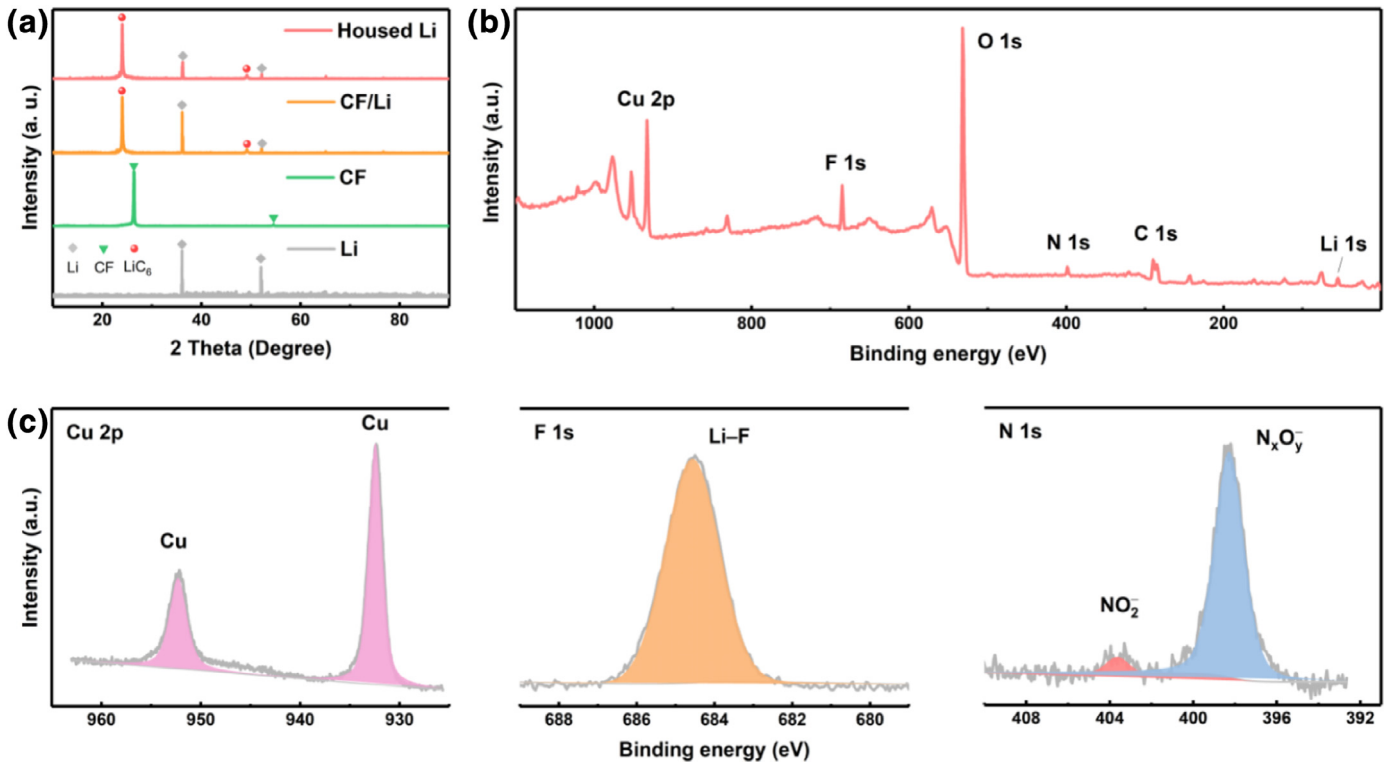

Fig. 3. Component characterizations of housed Li. (a) XRD patterns of Li, CF, CF/Li, and housed Li; (b) X-ray photoelectron spectroscopy of solid electrolyte layer; (c) The Cu 2*p*, N 1*s* and F 1*s* spectra of solid electrolyte layer.

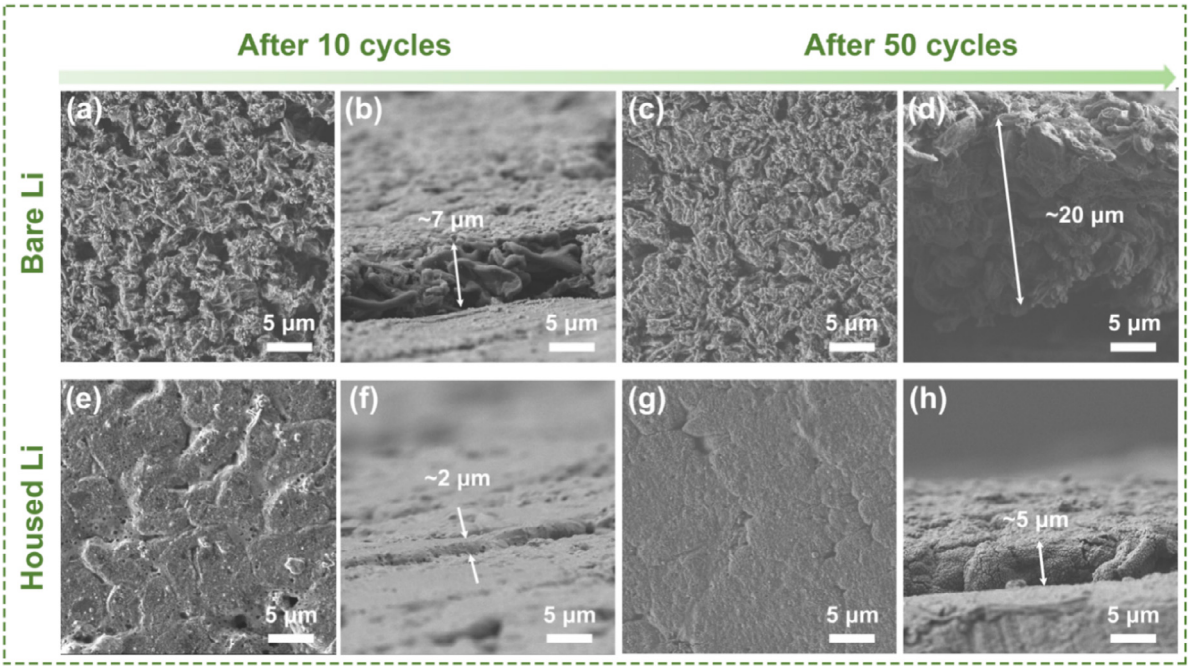

Fig. 4. Top-view and cross-sectional SEM images of cycled Li in Li | Li symmetric cell at 1.0 mA cm^{-2} and 1.0 mAh cm^{-2}. Bare Li after (a, b) 10 cycles and (c, d) 50 cycles. Housed Li after (e, f) 10 cycles and (g, h) 50 cycles.

layer in housed Li contributes to rapid charge transfer and electrochemical activation favors the mature of solid electrolyte layer. Inner CF matrix also plays vigorous role in providing highways for ion/electron transmission to reduce the resistance.

The housed Li is further evaluted in full cells. Housed Li | $LiFePO_4$ coin cell displays a high reversible capacity of 135 mAh g^{-1} with high capacity retention (>95%) at 1.0 C for 500 cycles (Fig. 5a, b), which is much better than bare Li (100 mAh g^{-1} after 238 cycles), SE/Li (100 mAh g^{-1} after 295 cycles), and CF/Li (100 mAh g^{-1} after 370 cycles). The morphology evolution of anodes affords a corroborating evidence. Flat surface and integral cross section are maintained after 100 cycles on house Li, but broken and uneven morphology is exhibited by bare Li (Fig. S9, Supporting Information). When replacing the FEC/$LiNO_3$ electrolyte

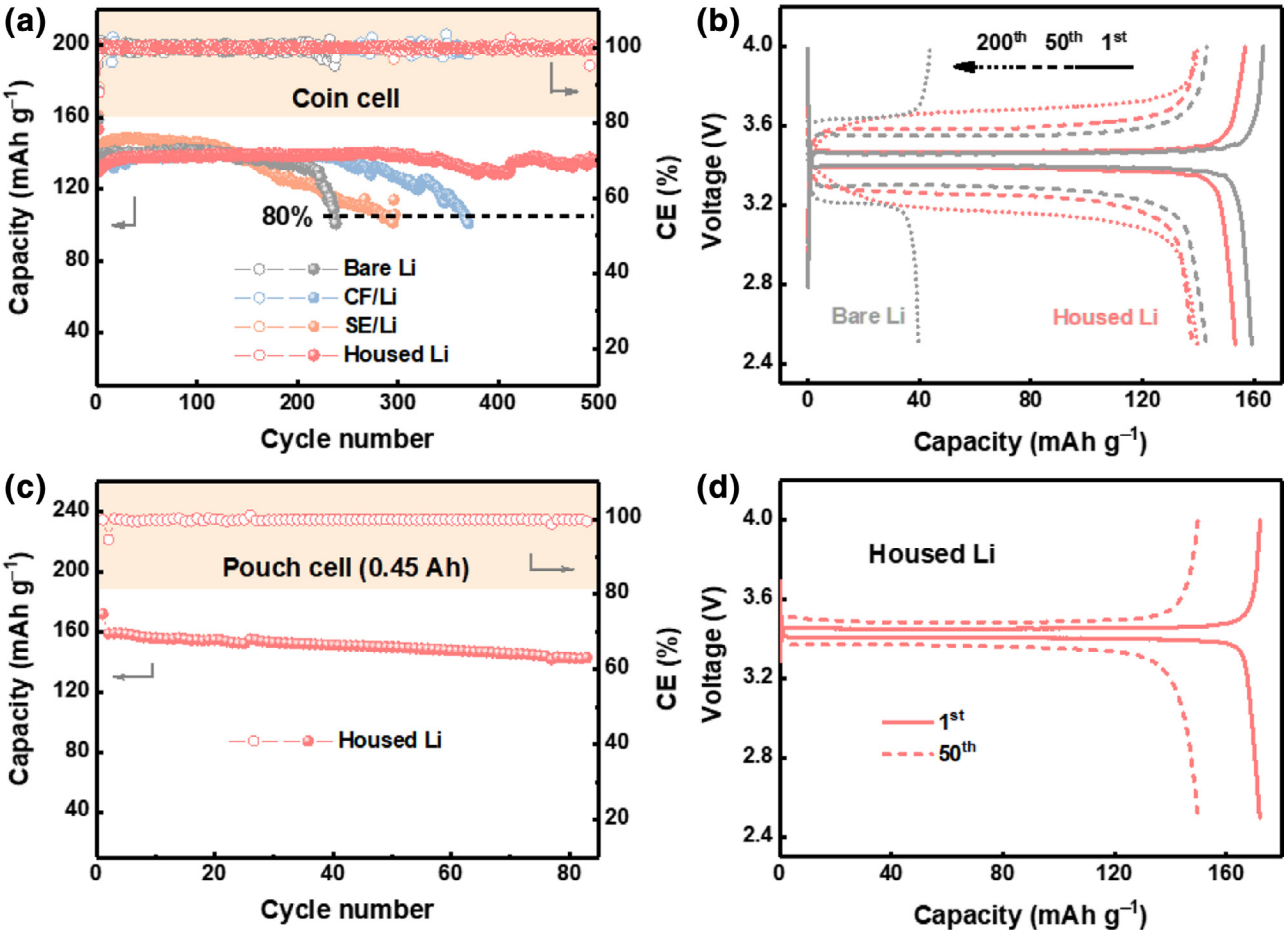

Fig. 5. Cycling stability of full cells with different anodes. Maintained capacity, coulombic efficiency and corresponding voltage profiles in (a, b) coin cell (cycling at 1.0 C after one cycle at 0.1 C) and (c, d) pouch cell (cycling at 0.5 C after one cycle at 0.05 C).

with a commercial carbonate electrolyte (1.0 M $LiPF_6$ in EC/DEC), similar cycling trend is observed (Fig. S10, Supporting Information). The cell with housed Li gains a prolonged lifespan of 225 cycles, whereas the cell with bare Li exhibits a short lifespan of 150 cycles at the same capacity retention of 80%.

Towards practical application, a 0.45 Ah housed Li | $LiFePO_4$ pouch cell with stacked electrodes was assembled (Fig. S11, Supporting Information) and test at 0.5 C rate. Remarkably, the corresponded current (0.152 A), which is far greater than that in coin cell, can lead to a worse non-uniform current density distribution on the electrode. As shown in Fig. 5(c, d), the cells with housed Li exhibit a reversible capacity of 143 mAh cm^{-2} and a high capacity retention of 85% after 80 cycles, demonstrating a superior stability in practical application.

A housed Li anode possessing upper solid electrolyte layer and bottom CF matrix is constructed. Based on aforementioned results, this housed Li can effectively eliminate Li dendrites and well confine volume change, and thus exhibits superior stability and prolonged cycling life in Li | Li symmetrical cell and Li | $LiFePO_4$ full cell.

These impressive electrochemical performances are explained from two aspects: (1) Reasonable combination of ion/electron channels. When nonuniform Li ion flux reaches the anode, it firstly passes through a solid electrolyte layer with high ion conductivity and outstanding mechanical stability, and thus is accelerated and homogenized. Subsequently, this uniform ion flux enters into the porous matrix with superior electron conductivity, rapidly obtaining electrons and depositing without Li dendrite. Conclusively, small polarization of 60 mV for housed Li after 1850 h (250 mV for bare Li after 1600 h at 0.5 mA cm^{-2}) is displayed. (2) Stable structure. The solid electrolyte layer, covering the surface of Li, effectively insulates metallic Li from the electrolyte, reducing unnecessary consumption of active materials and electrolyte. The inner matrix not only affords enough space for accommodating Li metal but also guarantees the integral structure from collapsing, significantly confining volume expansion (a dead Li layer with 5 μm for housed Li but 20 μm for bare Li after 50 cycles). Thanks to the protection of upper solid electrolyte layer, matrix successfully overcomes its inevitable defect, i.e., high active surface area causes copious SEI formation/side reaction during cycling. In return, stable structure maintained by matrix gently jacks up the SE without breaking. They both contribute to the high capacity retention (>95% after 500 cycles) in housed Li | $LiFePO_4$ full cells.

Furthermore, the fabrication method developed herein involves roll press and solution treatment, which are of the potential to be practically applied. On one hand, this preparation process is operable and facile at room temperature, while other thermal infusion method must operate at high temperature (more than 180 °C) and may induce a potential safety hazard [47–50]. On the other hand, the fabrication of housed Li is compatible to roll to roll large-scale and continuous fabrication processing, paving the way for industrial production. Therefore, based on the facile fabrication and superior role in extending the lifespan of LMBs, the strategy proposed here can present fresh insights into the practical applications of Li metal anode in LMBs.

4. Conclusions

A housed composite Li anode with rapid ion/electron transport channels and stable structure was designed. The carbon fiber matrix and solid electrolyte layer are integrated into one Li metal anode through the facile roll press and solution-based methods. The upper solid electrolyte layer protects Li metal from the corrosive electrolyte and promotes homogeneous Li ion distribution, while bottom CF matrix with stable structure affords enough voids and electron highway for Li ion diffusion. As a result, both dendrites and volume expansion are significantly inhibited. The cells using housed Li present prolonged lifetime (1850 h at 0.5 mA cm^{-2} and 950 h at 1.0 mA cm^{-2}) in Li | Li symmetrical cell and high capacity retention (>95% after 500 cycles in coin cell and 85% after 80 cycles in pouch cell) in Li | $LiFePO_4$ full cell further demonstrates the superior stability of housed Li. The alliance of solid electrolyte and matrix is a promising strategy to achieve stable and safe Li metal anodes for LMBs with high energy density.

Conflicts of interest

There are no conflicts to declare.

Acknowledgments

This work was supported by the National Key Research and Development Program (2016YFA0202500, 2015CB932500, and 2016YFA0200102), the National Natural Science Foundation of China (21676160, 21825501, 21805161, and 21808125), and China Postdoctoral Science Foundation (2017M620773, 2018M631480, and BX201700125).

Supplementary materials

Supplementary material associated with this article can be found, in the online version, at doi:10.1016/j.jechem.2018.11.016.

References

[1] V. Etacheri, R. Marom, R. Elazari, G. Salitra, D. Aurbach, Energy Environ. Sci. 4 (2011) 3243–3262.
[2] A. Manthiram, S.H. Chung, C.X. Zu, Adv. Mater. 27 (2015) 1980–2006.
[3] X.B. Cheng, R. Zhang, C.Z. Zhao, Q. Zhang, Chem. Rev. 117 (2017) 10403–10473.
[4] B. Liu, J.G. Zhang, W. Xu, Joule 2 (2018) 833–845.
[5] D.C. Lin, Y.Y. Liu, Y. Cui, Nat. Nanotech. 12 (2017) 194–206.
[6] S.J. Park, J.Y. Hwang, C.S. Yoon, H.G. Jung, Y.K. Sun, ACS Appl. Mater. Interfaces 10 (2018) 17985–17993.
[7] X.B. Cheng, C. Yan, X.Q. Zhang, H. Liu, Q. Zhang, ACS Energy Lett. 3 (2018) 1564–1570.
[8] R. Xu, X.Q. Zhang, X.B. Cheng, H.J. Peng, C.Z. Zhao, C. Yan, J.Q. Huang, Adv. Funct. Mater. 28 (2018) 1705838.
[9] X. Xu, S. Wang, H. Wang, C. Hu, Y. Jin, J. Liu, H. Yan, J. Energy Chem. 27 (2018) 513–527.
[10] J. Cui, T.-G. Zhan, K.-D. Zhang, D. Chen, Chin. Chem. Lett. 28 (2017) 2171–2179.
[11] L. Wang, Z. Zhou, X. Yan, F. Hou, L. Wen, W. Luo, J. Liang, S.X. Dou, Energy Storage Mater. 14 (2018) 22–48.
[12] F. Wu, Y.-X. Yuan, X.-B. Cheng, Y. Bai, Y. Li, C. Wu, Q. Zhang, Energy Storage Mater. 15 (2018) 148–170.
[13] M. Rosso, T. Gobron, C. Brissot, J.N. Chazalviel, S. Lascaud, J. Power Sources 97–98 (2001) 804–806.
[14] C. Zhang, Z.J. Huang, W. Lv, Q.B. Yun, F.Y. Kang, Q.H. Yang, Carbon 123 (2017) 744–755.
[15] Z.W. Sun, S. Jin, H.C. Jin, Z.Z. Du, Y.W. Zhu, A.Y. Cao, H.X. Ji, L.J. Wan, Adv. Mater. 30 (2018) 1800884.
[16] C.P. Yang, Y.G. Yao, S.M. He, H. Xie, E. Hitz, L.B. Hu, Adv. Mater. 29 (2017) 1702714.
[17] H. Ye, S. Xin, Y.X. Yin, J.Y. Li, Y.G. Guo, L.J. Wan, J. Am. Chem. Soc. 139 (2017) 5916–5922.
[18] Z.Y. Lu, Z.G. Zhang, X.C. Chen, Q.X. Chen, F.H. Ren, M.Q. Wang, S.D. Wu, Z. Peng, D.Y. Wang, J.C. Ye, Energy Storage Mater. 11 (2018) 47–56.
[19] C. Zhang, W. Lv, G.M. Zhou, Z.J. Huang, Y.B. Zhang, R.Y. Lyu, H.L. Wu, Q.B. Yun, F.Y. Kang, Q.H. Yang, Adv. Energy Mater. 8 (2018) 1703404.
[20] Q. Li, S.P. Zhu, Y.Y. Lu, Adv. Funct. Mater. 27 (2017) 1606422.
[21] Z.G. Jiang, T.F. Liu, L.J. Yan, J. Liu, F.F. Dong, M. Ling, C.D. Liang, Z. Lin, Energy Storage Mater. 11 (2018) 267–273.
[22] H.S. Wang, D.C. Lin, Y.Y. Liu, Y.Z. Li, Y. Cui, Sci. Adv. 3 (2017) e1701301.
[23] W.G. Zhao, L.F. Zou, J.M. Zheng, H.P. Jia, J.H. Song, M.H. Engelhard, C.M. Wang, W. Xu, Y. Yang, J.G. Zhang, ChemSusChem 11 (2018) 2211–2220.
[24] Q. Pang, X. Liang, A. Shyamsunder, L.F. Nazar, Joule 1 (2017) 871–886.
[25] F. Ding, W. Xu, G.L. Graff, J. Zhang, M.L. Sushko, X.L. Chen, Y.Y. Shao, M.H. Engelhard, Z.M. Nie, J. Xiao, X.J. Liu, P.V. Sushko, J. Liu, J.G. Zhang, J. Am. Chem. Soc. 135 (2013) 4450–4456.
[26] H. Zhang, G.G. Eshetu, X. Judez, C.M. Li, L.M. Rodriguez-Martinez, M. Armand, Angew. Chem. Int. Ed. (2018). https://doi.org/10.1002/anie.201712702.
[27] X. Li, J.M. Zheng, M. Engelhard, D.H. Mei, Q.Y. Li, S.H. Jiao, N. Liu, W.G. Zhao, J.G. Zhang, W. Xu, ACS Appl. Mater. Interfaces 10 (2017) 2469–2479.
[28] J. Neuhaus, E. von, Harbou, H. Hasse, J. Power Sources 394 (2018) 148–159.
[29] X.L. Fan, L. Chen, X. Ji, T. Deng, S. Hou, J. Chen, J. Zheng, F. Wang, J.J. Jiang, K. Xu, C.S. Wang, Chem 4 (2018) 174–185.
[30] X.D. Ren, S.R. Chen, H. Lee, D.H. Mei, M.H. Engelhard, S.D. Burton, W.G. Zhao, J.M. Zheng, Q.Y. Li, M.S. Ding, M. Schroeder, J. Alvarado, K. Xu, Y.S. Meng, J. Liu, J.G. Zhang, W. Xu, Chem 4 (2018) 1877–1892.
[31] J.M. Zheng, J.A. Lochala, A. Kwok, Z.Q.D. Deng, J. Xiao, Adv. Sci. 4 (2017) 1700032.
[32] C.Z. Zhao, X.Q. Zhang, X.B. Cheng, R. Zhang, R. Xu, P.Y. Chen, H.J. Peng, J.Q. Huang, Q. Zhang, Proc. Natl. Acad. Sci. USA 114 (2017) 11069–11074.
[33] C. Yan, X.B. Cheng, Y. Tian, X. Chen, X.Q. Zhang, W.J. Li, J.Q. Huang, Q. Zhang, Adv. Mater. 30 (2018) 1707629.
[34] X.Q. Zhang, X. Chen, R. Xu, X.B. Cheng, H.J. Peng, R. Zhang, J.Q. Huang, Q. Zhang, Angew. Chem. Int. Ed. 56 (2017) 14207–14211.
[35] Q. Zhao, Z.Y. Tu, S.Y. Wei, K.H. Zhang, S. Choudhury, X.T. Liu, L.A. Archer, Angew. Chem. Int. Ed. 57 (2018) 992–996.
[36] J.W. Ju, Y.T. Wang, B.B. Chen, J. Ma, S.M. Dong, J.C. Chai, H.T. Qu, L.F. Cui, X.X. Wu, G.L. Cui, ACS Appl. Mater. Interfaces 10 (2018) 13588–13597.
[37] D.W. McOwen, S.M. Xu, Y.H. Gong, Y. Wen, G.L. Godbey, J.E. Gritton, T.R. Hamann, J.Q. Dai, G.T. Hitz, L.B. Hu, E.D. Wachsman, Adv. Mater. 30 (2018) 1707132.
[38] W.H. Meyer, Adv. Mater. 10 (1998) 439–448.
[39] Z.Z. Zhang, Y.J. Shao, B. Lotsch, Y.S. Hu, H. Li, J. Janek, L.F. Nazar, C.W. Nan, J. Maier, M. Armand, L.Q. Chen, Energy Environ. Sci. 11 (2018) 1945–1976.
[40] D.C. in, Y.Y. Liu, W. Chen, G.M. Zhou, K. Liu, B. Dunn, Y. Cui, Nano Lett 17 (2017) 3731–3737.
[41] S.S. Chi, Y.C. Liu, N. Zhao, X.X. Guo, C.W. Nan, L.Z. Fan, Energy Storage Mater. (2018). https://doi.org/10.1016/j.ensm.2018.1007.1004.
[42] Y.J. Shao, H.C. Wang, Z.L. Gong, D.W. Wang, B.Z. Zheng, J.P. Zhu, Y.X. Lu, Y.S. Hu, X.X. Guo, H. Li, X.J. Huang, Y. Yang, C.W. Nan, L.Q. Chen, ACS Energy Lett. 3 (2018) 1212–1218.
[43] T.T. Zuo, X.W. Wu, C.P. Yang, Y.X. Yin, H. Ye, N.W. Li, Y.G. Guo, Adv. Mater. 29 (2017) 1700389.
[44] D. Aurbach, E. Pollak, R. Elazari, G. Salitra, C.S. Kelley, J. Affinito, J. Electrochem. Soc. 156 (2009) A694–A702.
[45] L. Zhang, M. Ling, J. Feng, L.Q. Mai, G. Liu, J.H. Guo, Energy Storage Mater. 11 (2018) 24–29.
[46] C.Z. Zhao, X.B. Cheng, R. Zhang, H.J. Peng, J.Q. Huang, R. Ran, Z.H. Huang, F. Wei, Q. Zhang, Energy Storage Mater. 3 (2016) 77–84.
[47] R. Zhang, X. Chen, X. Shen, X.Q. Zhang, X.R. Chen, X.B. Cheng, C. Yan, C.Z. Zhao, Q. Zhang, Joule 2 (2018) 764–777.
[48] Y. Zhang, C.W. Wang, G. Pastel, Y.D. Kuang, H. Xie, Y.J. Li, B.Y. Liu, W. Luo, C.J. Chen, L.B. Hu, Adv. Energy Mater. 8 (2018) 1800635.
[49] L.L. Lu, Y. Zhang, Z. Pan, H.B. Yao, F. Zhou, S.H. Yu, Energy Storage Mater. 9 (2017) 31–38.
[50] Y.L. Wang, Y.B. Shen, Z.L. Du, X.F. Zhang, K. Wang, H.Y. Zhang, T. Kang, F. Guo, C.H. Liu, X.D. Wu, W. Lu, L.W. Chen, J. Mater. Chem. A 5 (2017) 23434–23439.